The Astrophysical Journal, 951:20 (7pp), 2023 July 1 https://doi.org/10.3847/1538-4357/acd248

Constraints on Undetected Long-period Binaries in the Known Pulsar Population

Megan L. Jones[1], David L. Kaplan[1], Maura A. McLaughlin[2,3], and Duncan R. Lorimer[2,3]
[1] Center for Gravitation, Cosmology and Astrophysics, Department of Physics, University of Wisconsin-Milwaukee, Milwaukee, WI 53201, USA
megan.jones@nanograv.org
[2] Department of Physics and Astronomy, West Virginia University, P.O. Box 6315, Morgantown, WV 26506, USA
[3] Center for Gravitational Waves and Cosmology, West Virginia University, Chestnut Ridge Research Building, Morgantown, WV 26505, USA
Received 2022 August 25; revised 2023 April 19; accepted 2023 May 2; published 2023 June 29

Abstract

Although neutron star–black hole binaries have been identified through mergers detected in gravitational waves, a pulsar–black hole binary has yet to be detected. While short-period binaries are detectable due to a clear signal in the pulsar's timing residuals, effects from a long-period binary could be masked by other timing effects, allowing them to go undetected. In particular, a long-period binary measured over a small subset of its orbital period could manifest via time derivatives of the spin frequency incompatible with isolated pulsar properties. We assess the possibility of pulsars having unknown companions in long-period binaries and put constraints on the range of binary properties that may remain undetected in current data, but that may be detectable with further observations. We find that for 35% of canonical pulsars with published higher-order derivatives, the precision of measurements is not enough to confidently reject binarity (period $\gtrsim$2 kyr), and that a black hole binary companion could not be ruled out for a sample of pulsars without published constraints if the period is >1 kyr. While we find no convincing cases in the literature, we put more stringent limits on orbital period and longitude of periastron for the few pulsars with published higher-order frequency derivatives ($n \geqslant 3$). We discuss the detectability of candidates and find that a sample pulsar in a 100 yr orbit could be detectable within 5–10 yr.

Unified Astronomy Thesaurus concepts: Binary pulsars (153); Black holes (162)

1. Introduction

Pulsar–black hole (BH) binaries have been described as the "holy grail of astrophysics" (Faucher-Giguère & Loeb 2011); the discovery of such a system could reveal a wealth of information on stellar evolution and strong gravity. Although the exact number is highly uncertain, predictions range from a few to roughly 100 such binaries existing in the Galaxy (Lipunov et al. 2005; Lorimer & Kramer 2012; Shao & Li 2018). While no pulsar–BH binaries are yet known, large-scale pulsar surveys with the Square Kilometre Array (SKA) are predicted to increase the known pulsar population to 30,000 sources, 3000 of which are expected to be recycled pulsars (Keane et al. 2015), greatly increasing the likelihood of discovering exotic pulsar binaries such as these.

Sigurdsson (2003) outlines two formation scenarios for a pulsar–BH binary in the Galactic field. (1) The system starts as a binary consisting of two massive stars. The primary, more-massive star explodes, forming a BH with the system remaining bound. The secondary, less-massive star then explodes as a supernova, leaving behind a canonical pulsar in a wide orbit. A possible example of a progenitor to such a system is VFTS 243, which hosts a BH ($M_{\rm BH} > 9\ M_\odot$) in a $\sim$10 days orbit with a 25 $M_\odot$ O-type star (Shenar et al. 2022). (2) The pulsar would form first in a tighter binary, outlined in more detail by Sipior et al. (2004). Both progenitor main-sequence stars would be just below the mass threshold to form a BH and would need to be close enough for mass transfer. The neutron star progenitor (i.e., the primary star) would lose enough mass to the secondary star such that the secondary reaches the threshold of BH formation with the primary retaining enough mass to become a neutron star. Sipior et al. (2004) assume that the secondary's mass gain shortens its evolutionary timescale in accordance with the mass gained, while the primary's lifetime is not extended by mass loss. After the primary forms a neutron star, the two stars need to stay close enough for a second round of mass transfer, this time with the secondary losing mass to the newly formed neutron star. After this second period of mass transfer, the system would contain a recycled, millisecond pulsar (MSP) that will remain bound following the subsequent formation of the BH (Tauris et al. 2012). High-mass companions that have yet to become BHs could be detected via their optical emission (Igoshev & Perets 2019; Antoniadis et al. 2020; Antoniadis 2021).

The emergence of multimessenger astronomy has led to additional focus on a range of relativistic binaries incorporating neutron stars (e.g., Margutti & Chornock 2021). The LIGO/Virgo experiment has identified several gravitational wave sources consistent with the merger of a neutron star with a stellar-mass BH (e.g., Abbott et al. 2020a, 2020b), but a local pulsar–BH binary has yet to be detected at any orbital period. Pol et al. (2021) predict the number of potentially detectable short-period binaries ($P_b \leqslant 10$ days) in the Galaxy based on LIGO/Virgo estimates of event-based and population-based merger rates, finding a range between $\sim$1 and $\sim$13 detectable binaries. Here, in contrast, we investigate the possibility of a long-period binary ($P_b \lesssim 2$ kyr) hiding in the known pulsar population.

The ATNF Pulsar catalog v1.65 (PSRCAT;[4] Manchester et al. 2005) lists $\sim$3000 rotation-powered pulsars, $\sim$10% of which are known to be in binary systems. The longest "closed" orbit (with a data span longer than the binary period) listed is

[4] https://www.atnf.csiro.au/research/pulsar/psrcat/

5.3 yr (PSR J1638−4725; Lorimer et al. 2006); however, longer-period binaries have been identified through anomalous timing behavior. PSR J2032+4127 is in a highly eccentric orbit ($e = 0.978$) with a 40−50 yr period (Lyne et al. 2015; Ho et al. 2017). PSR B1620−26 is in a hierarchical triple system, orbiting a white dwarf with a 191 day period and a Jupiter-like planet with a ∼60 yr period (Thorsett & Arzoumanian 1999). PSR J1024–0719 is in a long-period binary orbit with a low-mass main-sequence star, identified via an unusually low-spin-period derivative; estimates on the orbital period are from 0.2–20 kyr (Bassa et al. 2016; Kaplan et al. 2016). The discovery of previously undetected long-period binary companions could explain anomalous timing behavior in other systems. Such a system could also help in understanding varied formation channels for neutron star binaries. This work is particularly timely given modern optical surveys and greatly increased pulsar timing programs through instruments like the Canadian H I Mapping Experiment (CHIME; CHIME/Pulsar Collaboration et al. 2021), the upgraded Molonglo Observatory Synthesis Telescope (UTMOST; Lower et al. 2020), and the future Deep Synoptic Array (DSA-2000; Hallinan et al. 2019).

The pulsar timing model characterizes time delays and effects in the data, fitting more parameters depending on the complexity of the system (Lorimer & Kramer 2012). If a particular effect is unmodeled, its resulting delays can be absorbed by other fit parameters, with the power reduced by this fitting quantified by the transmission function (e.g., Blandford et al. 1984). While short-period binaries would be detectable due to a clear periodic signal in the timing residuals, effects from a long-period binary could be masked by other timing delay effects (e.g., pulse spin-down and timing noise), allowing them to go undetected (e.g., Bassa et al. 2016; Kaplan et al. 2016). A long-period binary measured over comparably short timescales that is unaccounted for in the timing model could instead be fit out through a sum of polynomial terms (i.e., frequency derivatives).

In this paper, we assess the possibility of unknown long-period pulsar binaries in the pulsar catalog. We find no particularly convincing cases, and put constraints on the range of binary properties that may remain undetected in current data, but that may be detectable with further observations. We derive relations to known pulsar parameters to constrain possible hidden systems in Section 2. We put limits on orbital period and companion mass using the pulsar magnetic field and published constraints on frequency derivatives while incorporating a transmission function to account for power loss to other parameters in the timing model in Section 3. We discuss the detectability of candidates and plans for future candidate confirmation in Section 4.

2. Method

For an apparently isolated pulsar, the time-dependent phase of the pulse due to spin-down can be expressed as

$$\begin{aligned}\phi(t) &= f(t - t_0) + \frac{1}{2}\dot{f}(t - t_0)^2 + \ldots \\ &= \sum_{n=0}^{\infty} \frac{f_n}{(n+1)!}(t - t_0)^{(n+1)}, \end{aligned} \tag{1}$$

where t and t_0 are the current and reference times respectively, and f_n is the nth timing frequency derivative (e.g., Lorimer & Kramer 2012). The inclusion of a binary model adds additional terms to the phase, with the binary model amplitude characterized as $\propto (a/c)/P_b$ where a is the semimajor axis of the binary orbit and P_b is the binary period. The amplitude of binary motion will be quite small as binary period increases, making its effect on pulsar timing residuals harder to detect.

Any timing parameters that are present but unmodeled in the data will have power absorbed by other parameters in the model; depending on the scale and shape of the residuals due to a particular effect, residuals due to that parameter may be completed absorbed. This absorption not only removes traces of this effect, but also incorrectly skews other parameters in the timing model to account for this unmodeled effect. In the case of unmodeled binary motion, a sufficiently small binary amplitude may be completely absorbed by other effects, like pulse spin-down and timing noise. Here we discuss the most likely effects that may absorb the unmodeled binary amplitude.

2.1. Intrinsic Timing Variations

The frequency derivatives can contain contributions from both deterministic and stochastic variations for an isolated pulsar. For instance, there are expected to be deterministic frequency derivatives intrinsic to the pulsar arising from magnetic dipole radiation (i.e., pulsar spin-down). While f_1 due to spin-down can typically be easily measured via timing, this is usually only possible for f_2 for very young pulsars due to their comparatively higher f_2 values. For other pulsars, we can predict f_2 due to dipole radiation as

$$f_{2;\mathrm{d}} = n_b \frac{f_1^2}{f_0}, \tag{2}$$

where n_b is the braking index; here we assume the canonical value $n_b = 3$ (e.g., Lorimer & Kramer 2012; Espinoza et al. 2017), although actual measurements of young pulsars typically find smaller values (e.g., Chen & Li 2006; Parthasarathy et al. 2019). Higher-order spin-down terms can be calculated by taking more derivatives of this relation with respect to f_0 (Parthasarathy et al. 2019).

Stochastic spin-down variations known as "timing noise"—often referred to as "red noise" because of its spectral content (e.g., Goncharov et al. 2021)—can be modeled in a variety of ways, including power-law noise processes (e.g., Lasky et al. 2015). However, it can also be modeled via a polynomial basis function, leading to additional contributions to f_2 and other terms. Like dipole spin-down, this effect is typically stronger in younger pulsars.

There have been numerous analyses characterizing timing noise in the literature. Arzoumanian et al. (1994) defined the timing stability parameter as

$$\Delta_T = \log_{10}\left(\frac{|f_2|}{6f_0}T^3\right), \tag{3}$$

where the nominal observation length is $T = 10^8$ s, giving the commonly reported quantity Δ_8 characterizing the strength of the timing noise as essentially the logarithm of the anticipated rms timing noise as parameterized by f_2.

Shannon & Cordes (2010) asserted the need for more robust diagnostics to characterize timing noise. After a second-order fit for f_0 and f_1, the authors calculated the postfit rms σ_{TN}, which is assumed to be due to timing noise, through maximum

likelihood analysis as

$$\sigma_{\rm TN}(\mu s) = \exp(C) f_0^{\alpha} \left| \frac{f_1}{10^{-15}\, s^{-2}} \right|^{\beta} T_{\rm yr}^{\gamma}, \quad (4)$$

where $T_{\rm yr}$ is the observing time in years, and the best-fit parameters are $C = 2.0 \pm 0.4$, $\alpha = -0.9 \pm 0.2$, $\beta = 1.00 \pm 0.05$, and $\gamma = 1.9 \pm 0.2$.

Parthasarathy et al. (2019) performed a a linear least-squares regression analysis assuming a 10 yr timing baseline to fit the timing noise metric

$$\sigma_{\rm TN}(\mu s) = f_0 |f_1|^b, \quad (5)$$

where $b = -0.9 \pm 0.2$ for canonical pulsars, which agrees with the relation found by Shannon & Cordes (2010) by rotational symmetry (Jankowski et al. 2018).

For convenience when assessing the full pulsar population, we combine Equation (4) with the standard expression for the dipolar magnetic field (Lorimer & Kramer 2012):

$$B = 3.2 \times 10^{19} \sqrt{\frac{|f_1|}{f_0^3}}, \quad (6)$$

to express the anticipated timing noise in terms of the measured f_0 and B

$$\sigma_{\rm TN}(\mu s) = 7.22\, f_0^{2.1} \left(\frac{B}{10^{12}\,{\rm G}} \right)^2 T_{\rm yr}^{1.9}. \quad (7)$$

Beyond the stochastic but continuous timing noise discussed above, pulsars can exhibit discontinuous changes in their spin evolution known as "glitches" (Radhakrishnan & Manchester 1969; Reichley & Downs 1969; Fuentes et al. 2017), and unseen glitches may contribute to incorrect estimates of timing noise or other variations in spin rate (e.g., Parthasarathy et al. 2020; Lower et al. 2021; Antonelli et al. 2023), especially in younger/more energetic pulsars. For instance, the finite sampling of timing programs could miss glitches, and these could to incorrect estimates of the braking index (Espinoza et al. 2017). Changes in the pulse shape (e.g., Singha et al. 2021) can also mimic stochastic timing variations. For the most part, the empirical timing noise relations given above likely include some small unmodeled glitches (Parthasarathy et al. 2019, 2020); larger glitches can be identified separately with sufficient timing cadence.

2.2. Extrinsic Timing Variations

Torque variations, whether inside the neutron star or in the magnetosphere (Antonelli et al. 2023) will contribute to higher spin derivatives of neutron stars. There also can be external causes for timing variations. For instance, changes in the interstellar dispersion (Lam et al. 2015; Jones et al. 2017) can contribute to timing noises. However, here we focus on the presence of an unmodeled binary companion.

When not explicitly characterized by the timing model, unmodeled binary motion will introduce pulse residuals represented as sinusoids (for circular orbits); however, if $T \ll P_b$ then the residuals can instead be modeled as pulse frequency derivatives (Joshi & Rasio 1997). These derivatives can be expressed via Doppler shifts (and higher-order terms)

$$f_{n;b} = \left(\frac{2\pi G \tilde{M}}{P_b c^3} \right)^{1/3} \left(\frac{f_0}{n!} \right) \left(\frac{-2\pi}{P_b} \right)^n \sin\left(\omega + \frac{n\pi}{2} \right) \sin i, \quad (8)$$

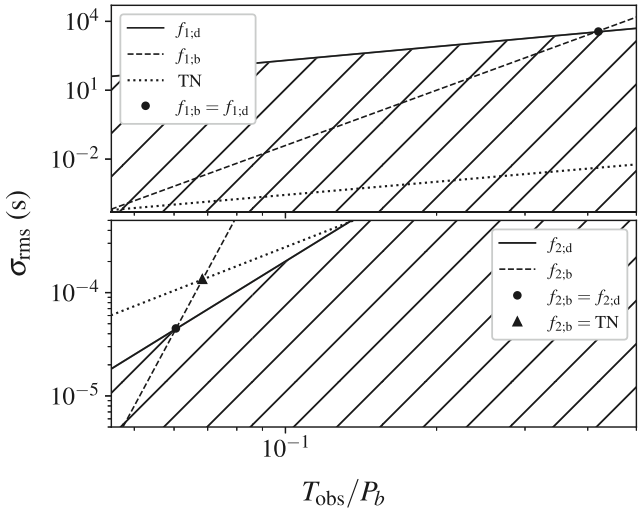

Figure 1. Induced rms residuals over observation span T for various effects. We assume $f_0 = 10$ Hz, $f_1 = 10^{-15}$ Hz/s, $B = 3.2 \times 10^{10}$ G, f_2 calculated using Equation (2), $M_{\rm BH} = 10\, M_\odot$, and P_b=100 yr. The top panel shows the comparison for f_1 while the bottom panel compares different contributions to f_2; a comparison to timing noise can be seen for both. The hatched regions show where residuals due to an unmodeled circular, edge-on binary companion will be overwhelmed by spin-down. The timing residuals from f_1 due to binary motion $f_{1;b}$ surpass those from f_1 due to dipole radiation $f_{1;d}$ around $\sim 0.4 P_b$, whereas those from $f_{2;b}$ surpass those from $f_{2;d}$ after $\sim 0.06 P_b$, making the search for a binary using f_2 more feasible than using f_1.

where $\tilde{M} = M_{\rm BH}^3/(M_{\rm BH} + M_P)^2$ with $M_{\rm BH}$ as the BH mass, M_P is the pulsar mass, ω is the longitude of periastron, and i is the binary inclination (e.g., Bhattacharyya & Nityananda 2008). This expression for $f_{n;b}$ can be used with Equation (1) to calculate the induced rms timing residuals $\sigma_{\rm rms} \approx \langle \Delta\phi(t)^2 \rangle^{1/2}/f_0$. Note that Equation (8) assumes a circular binary for simplicity, whether or not this is a good physical assumption; given the formation mechanisms discussed earlier, we would likely not expect a circular binary (e.g., DeCesar et al. 2015). An eccentric system can be straightforwardly approximated by adding an additional eccentricity factor $\epsilon = (1 + e\cos(\lambda))/(1 - e^2)$, where λ is the longitude of the companion from pericenter (Joshi & Rasio 1997).

For all pulsars, we specifically look for canonical sources that are not in a known binary and are not associated with a globular cluster, as cluster dynamics could introduce their own frequency derivative components (e.g., Phinney 1993). While present, contributions to f_2 due to Shklovskii acceleration, Galactic motion, and differential acceleration will not sufficiently contribute to the frequency derivatives for canonical pulsars considered here, but are likely relevant effects for MSPs (Shklovskii 1970; Guillemot et al. 2016; Liu et al. 2018; Pathak & Bagchi 2021).

2.3. Intrinsic versus Extrinsic Frequency Derivatives

When looking for unmodeled binary motion (Equation (8)), we must compare the expected frequency derivatives from such binaries to those expected from intrinsic sources (spin-down and timing noise, to start). A comparison of the induced timing residuals over time for dipole radiation, intrinsic timing noise, and an unmodeled binary can be seen in Figure 1. For the first frequency derivative, f_1 due to a binary would be overwhelmed by spin-down effects (Lamb & Lamb 1976, and Figure 1). We therefore focus on the second derivative f_2 as it is the first term

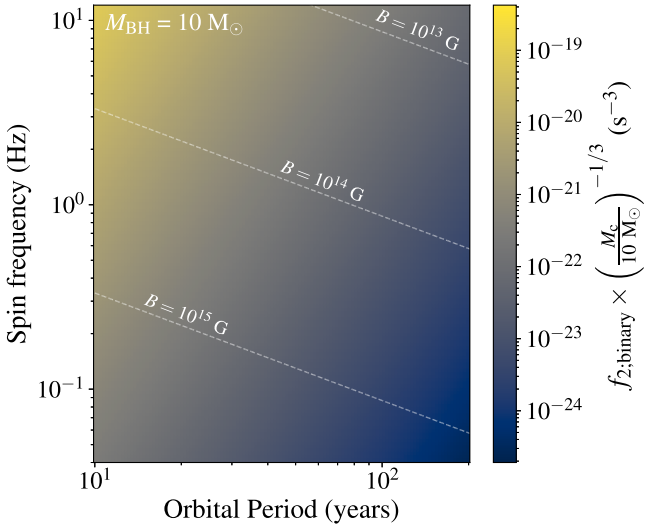

Figure 2. The f_2 induced for a circular binary for a range of spin and orbital periods. The black hole companion mass is assumed to be $10\,M_\odot$, and we assume the binary orbit is edge-on ($i = 90°$). The dashed lines represent the surface magnetic field B corresponding to a specific f_2 due solely to dipole radiation ($n_b = 3$). To use this for a particular pulsar with a single value of f_0 and B, any orbital period to the left of where that f_0 value crosses the appropriate B contour may be probed in binary searches. Following Equation (9), this suggests an upper limit on orbital period where longer periods will be hidden by magnetic field effects. The magnetic fields necessary to feasibly attribute unmodeled binary motion to dipole radiation are generally higher than would be expected for most canonical pulsars.

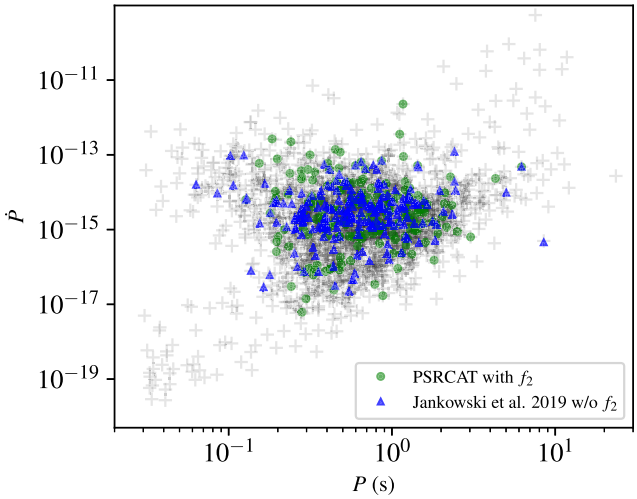

Figure 3. P–$\dot{P}$ diagram of identified candidates. The light gray crosses show all the known nonmillisecond pulsars ($P > 30$ ms) with published f_1 in PSRCAT. Unassociated isolated pulsars with published f_2 constraints are represented with green circles, and blue triangles show those observed by Jankowski et al. (2019) without a published constraint on f_2.

that is potentially larger than the dipole radiation contribution. For a binary to be detectable, the orbital period must be short enough that the induced timing residuals stand out with respect to other sources of timing offsets, but long enough that the binary motion is not obvious from the residuals (i.e., $T \ll P_b$). Predicted f_2 values for various spin frequencies and orbital periods can be seen in Figure 2 along with the necessary pulsar magnetic field to account for the induced f_2 due to a binary orbit.

3. Limits for Known Pulsars

Given the constraints on binary detectability via frequency derivatives as well as intrinsic timing effects, we determine an orbital parameter phase space in which we are sensitive for the known pulsar population. We will determine these limits on detectability through several methods in the next sections depending on the highest-order frequency derivative published for a given pulsar that meets these criteria.

3.1. Sample Selection

3.1.1. Pulsars without Higher-order Constraints

First, we use the calculated magnetic field as the upper limit for pulsars without published higher-order frequency derivatives to predict f_2 due to dipole radiation in the absence of a measured constraint; induced f_2 from binaries with periods above this limit will be overwhelmed by spin-down effects. Combining Equations (2) and (8) yields an upper limit constraint on orbital period

$$P_b^{7/3} \lesssim \frac{1}{n_b f_0^4}\left(\frac{\tilde{M}}{10\,M_\odot}\right)^{1/3}\left(\frac{B}{10^{15}\,{\rm G}}\right)^{-4}, \quad (9)$$

where P_b is in years (also see Figure 2). Because any induced f_2 for sources considered in this section will be unmodeled in the timing model, the signal due to the orbital frequency of the binary will be reduced by a factor characterized by the transmission function (Blandford et al. 1984; Madison et al. 2013; Hazboun et al. 2019). The transmission function quantifying the power absorbed due to spin-down, modeled as a quadratic function of time, goes as

$$\mathcal{T}_f \sim \left(\frac{T_{\rm obs}}{1.086\,P_b}\right)^6, \quad (10)$$

where $T_{\rm obs} < P_b$ for this equation, which is unitless, to hold (Jennings et al. 2020). By combining Equations (8) and (10) where $\sigma_{\rm rms} = \mathcal{T}_f \times \sigma_{f_2}$, we calculate the maximum f_2 that could evade detection over the given observation span $T_{\rm yr}$ in years using published timing residuals $\sigma_{\rm rms}$ in seconds and set a lower limit on orbital period

$$P_b \gtrsim 2.7\left(\frac{\tilde{M}}{10\,M_\odot}\right)^{0.04}\sigma_{\rm rms}^{-0.12}\,T_{\rm yr}^{1.08}. \quad (11)$$

3.1.2. Pulsars with Published Constraints on f_2

Next, we look at pulsars with published constraints on f_2. Again, we use the magnetic field to set an upper limit on possible orbital periods. We evaluate Equation (8) for the published f_2 to calculate the minimum orbital period that could be hidden for a given pulsar

$$\left(\frac{P_b}{100\ {\rm yr}}\right) \gtrsim \left(\frac{\tilde{M}}{10\,M_\odot}\right)^{1/7}\left(\frac{f_0}{1\ {\rm Hz}}\right)^{3/7}\left(\frac{f_2}{10^{-22}\ {\rm s}^{-2}}\right)^{-3/7}. \quad (12)$$

Periods shorter than this limit will induce a higher f_2 than the published constraint, and are therefore unphysical for that pulsar.

Table 1
Unassociated Pulsars with Published f_3 and/or f_4

	J1910+0517[a]	J1913+1330[b]	J1929+1357[a]
f_2 (s^{-2})	$7.5(6)\times10^{-24}$	$6(5)\times10^{-27}$	$1.00(2)\times10^{-23}$
f_3 (s^{-3})	$-1.8(3)\times10^{-31}$	$-6.9(3)\times10^{-33}$	$-4.2(4)\times10^{-31}$
f_4 (s^{-5})	$-2.6(3)\times10^{-38}$	$7(1)\times10^{-41}$	⋯
ω (rad)	⋯	0.11(6)	<0.52(3)
P_b (yr)	⋯	0.5(3)	>3.0(6)

Notes. Limits on orbital period and orientation based on published constraints on higher-order frequency derivatives for unassociated pulsars in PSRCAT. Signs on frequency derivatives due to a binary would need to alternate positive and negative or all be the same sign to be physical; therefore, an estimate on orbital parameters could not be made for PSR J1910+0517.
[a] Lyne et al. (2017).
[b] Bhattacharyya et al. (2018).

3.1.3. Candidates with Published f_3 and/or f_4

With the availability of higher-order frequency derivatives constraints, even more stringent limits on orbital parameters can be made. Comparing two frequency derivatives f_n and f_{n+1} gives a range of possible orbital periods and longitude of periastron

$$P_b = \left(\frac{-2\pi}{n+1}\right)\left(\frac{f_n}{f_{n+1}}\right)\cot\left(\omega + \frac{n\pi}{2}\right). \quad (13)$$

While two frequency derivatives can be used to constrain a possible range of values for P_b and ω, using three derivatives constrains this range of values to a single estimate for each. There are three unassociated pulsars in PSRCAT with higher-order frequency derivative constraints: PSR J1929+1357 has a published f_3 constraint (Lyne et al. 2017), whereas PSRs J1910+0517 and J1913+1330 have published constraints on both f_3 and f_4 (Lyne et al. 2017; Bhattacharyya et al. 2018). The more stringent limits on a possible binary in these systems are listed in Table 1.

Depending on the longitude of the binary with respect to the periastron, all successive frequency derivatives due to circular binary motion should have either like or alternating signs, as can be seen in Equation (8); this is not true for J1910+0517. Therefore it is unlikely that these two measurements are due to an unmodeled binary. However, this binary criterion is met for J1913+1330 and a more constrained orbital period can be determined. By comparing f_2, f_3, and f_4, we solve for a value of ω that gives a P_b that satisfies all three measurements. We find a possible orbital period of $P_b = 0.5 \pm 0.3$ yr with a longitude of periastron of $\omega = 0.11 \pm 0.06$ rad. Without a constrained f_4 for J1929+1357, we cannot solve for both P_b and ω, but can identify combinations of the period and longitude of periastron that agree with the published constraints on f_2 and f_3. A plot of these two limits can be seen in Figure 4.

It is worth noting that these three pulsars show time-variable emission and are categorized as rotating radio transients (RRATs). While constraints on binary parameters can be obtained using measured frequency derivatives, confirming companions may be difficult given the transient nature of these pulsars and the irregular timing of the pulses, although in some cases deeper observations may be able to reveal more regular emission (e.g., Mickaliger et al. 2018).

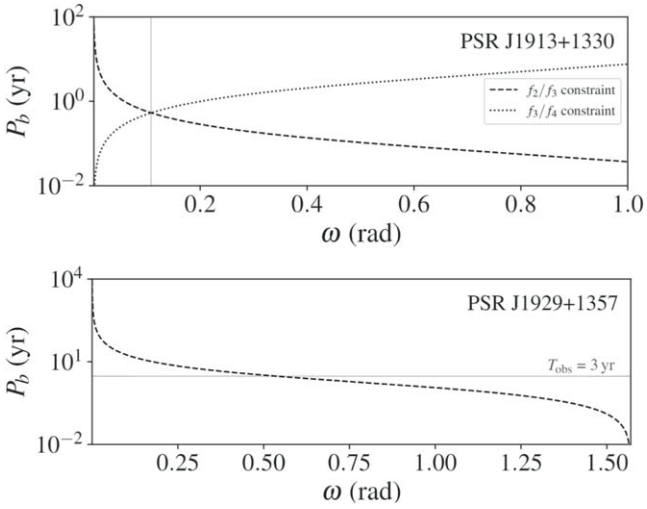

Figure 4. Limits on P_b as a function of longitude of periastron for PSRs 1913+1330 and 1929+1357. Using constraints on higher-order derivatives, we identify the range of combinations in longitude of periastron and orbital period that satisfy these constraints. In the top panel, J1913+1330 has published constraints up to f_4, which allows for more constrained orbital parameters compared to J1929+1357 in the bottom panel, which only has published derivatives up to f_3. The gray line in the bottom panel shows the timing baseline from Jankowski et al. (2019) for comparison as a lower limit on a potential binary period. Note that using the ratio of frequency derivatives cancels out the companion mass, causing the limits calculated here to be independent of mass.

3.2. Constraining Binaries within the Population

For pulsars with a published constraint on f_2, we apply our f_2-based limits to the full isolated pulsar population in PSRCAT. Due to the large number of isolated pulsars without a measured f_2 in PSRCAT, we focus on a subset of the population observed in Jankowski et al. (2019) without published f_2 measurements to ensure more uniform observations for the evaluation of the rms timing residuals and therefore calculate a lower limit on minimum orbital period using Equation (11). The range of spin periods and period derivatives for these two populations can be seen in Figure 3. To reduce the number of degrees of freedom, we assume the mean value of $2/\pi$ for $\sin(\omega + n\pi/2)$ for this analysis.

Comparing Equation (8) to the published frequency derivatives in both populations above, we predict the fraction of sources that could hide a binary with some minimum orbital period based on published constraints on the frequency derivative. Assuming a Poisson distribution for the anticipated percentage of pulsars hiding a binary, we calculate the probable ranges for the population fraction hiding binary companions with a given minimum orbital period. Ranges are given for pulsars both with and without a published f_2, seen in Figure 5. Note that these ranges are empirically derived from population parameters and are not physically motivated from binary formation.

By examining the percentage of pulsars with measured f_2 that could hide a binary with various orbital periods, we fit the following relation to our populations to yield an upper limit on the number of sources with orbital periods above a given minimum orbital period $P_{b;\min}$:

$$\log_{10} P_{b;\min} = \alpha + \beta x, \quad (14)$$

where x is the percentage of the population that could hide a corresponding $P_{b;\min}$ (in years). Applying a least-squares fit to

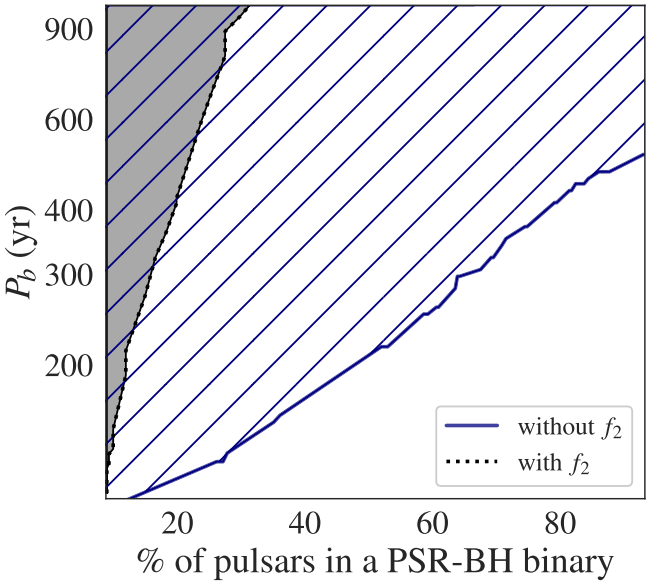

Figure 5. The percentage of isolated pulsars that could hide a pulsar–BH binary at a given orbital period, assuming the binary is edge-on with $M_{\rm BH} = 10\ M_\odot$. The shaded and hatched regions show where the likelihood level is within 95%. The gray region includes pulsars with a published f_2, while the blue hatched region shows pulsars without published higher-order frequency derivatives. As the percentage of pulsars with potential hidden binaries increases, the likelihood for a fixed period decreases. With the availability of higher-order frequency constraints, the probable region decreases substantially. For instance, for pulsars with a published f_2 and $P_b = 300$ yr, we can exclude that more than 10% of pulsars hide such a binary, while up to ∼60% of pulsars without f_2 could hide such a binary.

the 177 PSRCAT sources with a published f_2 finds $\alpha = 2.17(5)$ and $\beta = 3.2(2)$. Similarly, for the 158 sources without f_2 this fit yields $\alpha = 1.95(2)$ and $\beta = 0.99(5)$; with these values for α and β, we find ∼35% as an upper limit in our sample that could hide a binary with $P_{b;\rm min} \geqslant 200$ yr. Note that our analysis found 100% of pulsars in Jankowski et al. (2019) could hide a binary with a minimum orbital period of ∼1 kyr; therefore, Equation (14) breaks down when investigating minimum periods above this value without a constraint on f_2.

4. Discussion and Conclusions

Building on historical work, we developed relations between effects on measured parameters and unmodeled binary motion. Using published constraints on higher-order frequency derivatives, we identified a range of orbital periods and longitudes of periastron for one pulsar, and placed a more stringent constraint on these parameters for another pulsar. A third pulsar had published frequency derivatives that are not congruent with binary motion.

Using limits on orbital period, we found that a long-period binary could not be ruled out for roughly 30% of pulsars with nonzero f_2 constraints, and that binary periods greater than ∼1 kyr could not be ruled out for pulsars analyzed here without a constrained f_2. Sources that do not have published higher-order frequency derivatives may still produce measurable constraints on these derivatives with further timing, particular through high-cadence programs like CHIME and the future DSA-2000 (CHIME/Pulsar Collaboration et al. 2021; Hallinan et al. 2019). The lower limit on orbital period given an observing time $T_{\rm yr}$ and a detected f_2 due to a binary can be determined from

$$P_b \geqslant 5.89 \times 10^3 |f_{2;\rm b}|^{1/6} \left(\frac{T_{\rm yr}}{\sigma_{\rm toa}}\right)^{3/2}, \quad (15)$$

where $\sigma_{\rm toa} \propto \sigma_{\rm rms} S_\nu^{-1} \sqrt{W(P-W)}/P$, S_ν is the frequency-dependent flux, and W and P are the pulse width and period respectively (Lorimer & Kramer 2012). For example, a $10\ M_\odot$ binary companion in a 100 yr orbit with a pulsar having a 10 Hz spin frequency, 10 ms pulse width, and 100 mJy flux at 843 MHz would be detectable with monthly 30 minute observations in ∼5 yr assuming an instrument like UTMOST (Lower et al. 2020). With this observing strategy, higher-order derivatives like f_3 and f_4 would be detectable in ∼7 and ∼10 yr respectively.

However, we note that this analysis assumes that timing is performed with sufficient cadence to capture any glitches, and that any timing variations due to changes in pulse shape or interstellar dispersion are small. For the most part, the latter effects are only detectable for precision timing of millisecond pulsars (e.g., Jones et al. 2017) used for detecting gravitational waves, and are unlikely to be significant for younger, noisier pulsars considered here. Unmodeled glitches may set a floor for the detectability of any binary to the extent that they are not already included in the empirical timing noise models used above. In that case our analysis may be overly conservative, and so the true fraction of binaries that we cannot exclude could be lower than 30%.

Follow-up of candidates with Gaia, while excellent for shorter binary periods (Mingarelli et al. 2018), will heavily depend on binary orbital period and distance to the pulsar. For example, Andrews et al. (2022) utilize Data Release 3 astrometry to identify potential neutron star–BH binaries, with orbital periods of ∼0.9–3.8 yr. Gaia lists an upper limit of 40 yr on detectable orbits and therefore is not feasible for the orbital period ranges identified here, but could still be useful in finding stellar companions by identifying common proper motion pairs.

Unmodeled binary motion will cause a deviation from linear proper motion. Multiple observations over time with instruments like the Very Long Baseline Array and ngVLA could hypothetically track the proper motion over time; however, the motions described here will induce deviations in proper motion that are smaller than published measurement errors. For example, a pulsar with a proper motion of 10 mas yr^{-1} and a distance of 1 kpc in a 20 yr binary would see a change in proper motion of $\sim 10^{-5}$ mas yr^{-1} after 5 yr of observing. For this method to successfully follow up on candidates and complement timing constraints on proper motion in the line of sight, constraints on motion in the plane of the sky would require higher precision of $\sim 10^{-3}$–10^{-2} mas yr^{-1}.

Acknowledgments

The authors would like to thank Nihan Pol and Joseph Lazio for useful discussions and manuscript comments. The authors are members of the NANOGrav NSF Physics Frontiers Center (awards #1430284 and 2020265).

ORCID iDs

Megan L. Jones https://orcid.org/0000-0001-6607-3710
David L. Kaplan https://orcid.org/0000-0001-6295-2881
Maura A. McLaughlin https://orcid.org/0000-0001-7697-7422

Duncan R. Lorimer https://orcid.org/0000-0003-1301-966X

References

Abbott, B. P., Abbott, R., Abbott, T. D., et al. 2020a, ApJL, 892, L3
Abbott, R., Abbott, T. D., Abraham, S., et al. 2020b, ApJL, 896, L44
Andrews, J. J., Taggart, K., & Foley, R. 2022, arXiv:2207.00680
Antonelli, M., Basu, A., & Haskell, B. 2023, MNRAS, 520, 2813
Antoniadis, J. 2021, MNRAS, 501, 1116
Antoniadis, J., Chanlaridis, S., Gräfener, G., & Langer, N. 2020, A&A, 635, A72
Arzoumanian, Z., Nice, D. J., Taylor, J. H., & Thorsett, S. E. 1994, ApJ, 422, 671
Bassa, C. G., Janssen, G. H., Stappers, B. W., et al. 2016, MNRAS, 460, 2207
Bhattacharyya, B., Lyne, A. G., Stappers, B. W., et al. 2018, MNRAS, 477, 4090
Bhattacharyya, B., & Nityananda, R. 2008, MNRAS, 387, 273
Blandford, R., Narayan, R., & Romani, R. W. 1984, JApA, 5, 369
Chen, W. C., & Li, X. D. 2006, A&A, 450, L1
CHIME/Pulsar Collaboration, Amiri, M., Bandura, K. M., et al. 2021, ApJS, 255, 5
DeCesar, M. E., Ransom, S. M., Kaplan, D. L., Ray, P. S., & Geller, A. M. 2015, ApJL, 807, L23
Espinoza, C. M., Lyne, A. G., & Stappers, B. W. 2017, MNRAS, 466, 147
Faucher-Giguère, C.-A., & Loeb, A. 2011, MNRAS, 415, 3951
Fuentes, J. R., Espinoza, C. M., Reisenegger, A., et al. 2017, A&A, 608, A131
Goncharov, B., Reardon, D. J., Shannon, R. M., et al. 2021, MNRAS, 502, 478
Guillemot, L., Smith, D. A., Laffon, H., et al. 2016, A&A, 587, A109
Hallinan, G., Ravi, V., Weinreb, S., et al. 2019, BAAS, 51, 255
Hazboun, J. S., Romano, J. D., & Smith, T. L. 2019, PhRvD, 100, 104028
Ho, W. C. G., Ng, C. Y., Lyne, A. G., et al. 2017, MNRAS, 464, 1211
Igoshev, A. P., & Perets, H. B. 2019, MNRAS, 486, 4098
Jankowski, F., Bailes, M., van Straten, W., et al. 2019, MNRAS, 484, 3691
Jankowski, F., van Straten, W., Keane, E. F., et al. 2018, MNRAS, 473, 4436
Jennings, R. J., Cordes, J. M., & Chatterjee, S. 2020, ApJ, 904, 191
Jones, M. L., McLaughlin, M. A., Lam, M. T., et al. 2017, ApJ, 841, 125
Joshi, K. J., & Rasio, F. A. 1997, ApJ, 479, 948
Kaplan, D. L., Kupfer, T., Nice, D. J., et al. 2016, ApJ, 826, 86
Keane, E., Bhattacharyya, B., Kramer, M., et al. 2015, in Proc. of Advancing Astrophysics with the Square Kilometre Array (AASKA14), 215, 40
Lam, M. T., Cordes, J. M., Chatterjee, S., & Dolch, T. 2015, ApJ, 801, 130
Lamb, D. Q., & Lamb, F. K. 1976, ApJ, 204, 168
Lasky, P. D., Melatos, A., Ravi, V., & Hobbs, G. 2015, MNRAS, 449, 3293
Lipunov, V. M., Bogomazov, A. I., & Abubekerov, M. K. 2005, MNRAS, 359, 1517
Liu, X. J., Bassa, C. G., & Stappers, B. W. 2018, MNRAS, 478, 2359
Lorimer, D. R., Faulkner, A. J., Lyne, A. G., et al. 2006, MNRAS, 372, 777
Lorimer, D. R., & Kramer, M. 2012, Handbook of Pulsar Astronomy, Vol. 4 (Cambridge, UK: Cambridge Univ. Press)
Lower, M. E., Bailes, M., Shannon, R. M., et al. 2020, MNRAS, 494, 228
Lower, M. E., Johnston, S., Dunn, L., et al. 2021, MNRAS, 508, 3251
Lyne, A. G., Stappers, B. W., Freire, P. C. C., et al. 2017, ApJ, 834, 72
Lyne, A. G., Stappers, B. W., Keith, M. J., et al. 2015, MNRAS, 451, 581
Madison, D. R., Chatterjee, S., & Cordes, J. M. 2013, ApJ, 777, 104
Manchester, R. N., Hobbs, G. B., Teoh, A., & Hobbs, M. 2005, AJ, 129, 1993
Margutti, R., & Chornock, R. 2021, ARA&A, 59, 155
Mickaliger, M. B., McEwen, A. E., McLaughlin, M. A., & Lorimer, D. R. 2018, MNRAS, 479, 5413
Mingarelli, C. M. F., Anderson, L., Bedell, M., & Spergel, D. N. 2018, arXiv:1812.06262
Parthasarathy, A., Johnston, S., Shannon, R. M., et al. 2020, MNRAS, 494, 2012
Parthasarathy, A., Shannon, R. M., Johnston, S., et al. 2019, MNRAS, 489, 3810
Pathak, D., & Bagchi, M. 2021, NewA, 85, 101549
Phinney, E. S. 1993, in ASP Conf. Ser. 50, Structure and Dynamics of Globular Clusters, ed. S. G. Djorgovski & G. Meylan (San Francisco, CA: ASP), 141
Pol, N., McLaughlin, M., & Lorimer, D. 2021, arXiv:2109.04512
Radhakrishnan, V., & Manchester, R. N. 1969, Natur, 222, 228
Reichley, P. E., & Downs, G. S. 1969, Natur, 222, 229
Shannon, R. M., & Cordes, J. M. 2010, ApJ, 725, 1607
Shao, Y., & Li, X.-D. 2018, MNRAS, 477, L128
Shenar, T., Sana, H., Mahy, L., et al. 2022, NatAs, 6, 1085
Shklovskii, I. S. 1970, SvA, 13, 562
Sigurdsson, S. 2003, in ASP Conf. Ser. 302, Radio Pulsars, ed. M. Bailes, D. J. Nice, & S. E. Thorsett (San Francisco, CA: ASP), 391
Singha, J., Surnis, M. P., Joshi, B. C., et al. 2021, MNRAS, 507, L57
Sipior, M. S., Portegies Zwart, S., & Nelemans, G. 2004, MNRAS, 354, L49
Tauris, T. M., Langer, N., & Kramer, M. 2012, MNRAS, 425, 1601
Thorsett, S. E., & Arzoumanian, Z. 1999, in Pulsar Timing, General Relativity and the Internal Structure of Neutron Stars, ed. Z. Arzoumanian, F. Van der Hooft, & E. P. J. van den Heuvel (Amsterdam: Koninklijke Nederlandse Akademie van Wetenschappen), 73

The Astrophysical Journal, 955:81 (3pp), 2023 September 20 https://doi.org/10.3847/1538-4357/acf71e

Erratum: "Constraints on Undetected Long-period Binaries in the Known Pulsar Population" (2023, ApJ, 951, 20)

Megan L. Jones[1], David L. Kaplan[1], Maura A. McLaughlin[2,3], and Duncan R. Lorimer[2,3]
[1] Center for Gravitation, Cosmology and Astrophysics, Department of Physics, University of Wisconsin-Milwaukee, Milwaukee, WI 53201, USA; kaplan@uwm.edu
[2] Department of Physics and Astronomy, West Virginia University, P.O. Box 6315, Morgantown, WV 26506, USA
[3] Center for Gravitational Waves and Cosmology, West Virginia University, Chestnut Ridge Research Building, Morgantown, WV 26505, USA
Received 2023 August 21; revised 2023 September 5; published 2023 September 20

In the published article, we explored the presence of undetected long-period (where the orbital period is much greater than the data span) binaries in the existing pulsar catalog. These would be systems where binary motion was instead modeled as a series of secular frequency derivatives. While we did not identify any likely binary systems, we did set out a methodology for evaluating candidates based on their frequency derivatives and found that long-period ($\geqslant$2 kyr) binaries could be present in as much as 35% of the population based on observed period derivatives and limits.

However, we have identified an error in the derivation of a key equation of the published article. This does not change the conclusions qualitatively, but does alter some of the results for individual pulsars. Below we rederive the key equation of the published article, Equation (8), and update the results for PSRs J1910+0517, J1913+1330, and J1929+1357.

As described by Lange et al. (2001), the Römer delay for near-circular orbits

$$\Delta_R \approx x\left(\sin\Phi + \frac{\kappa}{2}\sin 2\Phi - \frac{\epsilon}{2}\cos 2\Phi\right), \tag{1}$$

where x is the projected size of the pulsar's semimajor axis, κ and ϵ are terms proportional to the eccentricity, and

$$\Phi(T) = n_b(T - T_{\rm asc}) \tag{2}$$

is the orbital phase (mean anomaly, to within a constant offset) as a function of time. Here $n_b = 2\pi/P_b$ is the orbital frequency for period P_b, and the time of the ascending node can be computed as

$$T_{\rm asc} = T_0 - \omega/n_b, \tag{3}$$

where T_0 is the time of periastron (also see Lorimer & Kramer 2012). Taking the circular case ($\epsilon = \kappa = 0$), we find

$$\Phi(T) = n_b\left(T - T_0 + \frac{\omega}{n_b}\right) = n_b(T - T_0) + \omega \tag{4}$$

and

$$\Delta_R = x\sin\left(n_b(T - T_0) + \omega\right). \tag{5}$$

We define $t = T - T_0$ and write the circular Römer delay as

$$\Delta_R(t) = x\sin(n_b t + \omega). \tag{6}$$

From this result, we can get the line-of-sight velocity,

$$v = \frac{d\Delta_R}{dt} = xn_b\cos(n_b t + \omega), \tag{7}$$

and acceleration,

$$a = \frac{d^2\Delta_R}{dt^2} = -xn_b^2\sin(n_b t + \omega). \tag{8}$$

Table 1
Comparison of Frequency Derivative Terms with Those from the Published Article

Order n	Term	Value	Jones et al. Value
1	$\dot{f}/f$	$(xn_b^2/c)\sin\omega$	$-(xn_b^2/c)\cos\omega$
2	$\ddot{f}/f$	$(xn_b^3/c)\cos\omega$	$-(xn_b^3/2c)\sin\omega$
3	$\dddot{f}/f$	$-(xn_b^4/c)\sin\omega$	$(xn_b^4/6c)\cos\omega$
4	$\ddddot{f}/f$	$-(xn_b^5/c)\cos\omega$	$(xn_b^5/24c)\sin\omega$

Note. The xn_b^{n+1}/c prefactor given in the published article is written differently but has the same magnitude.

This is the same as given in Equation (8.26) of Lorimer & Kramer (2012), although here we only give it for zero eccentricity. We can also identify further derivatives:

$$\begin{aligned}\frac{da}{dt} &= -xn_b^3\cos(n_b t+\omega)\\ \frac{d^2a}{dt^2} &= xn_b^4\sin(n_b t+\omega)\\ \frac{d^3a}{dt^3} &= xn_b^5\cos(n_b t+\omega),\end{aligned} \tag{9}$$

and so on. We then look at Joshi & Rasio (1997), where their Equation (3) states

$$\begin{aligned}\frac{\dot{f}}{f} &= -\frac{a}{c}\\ \frac{\ddot{f}}{f} &= -\frac{\dot{a}}{c}\\ \frac{\dddot{f}}{f} &= -\frac{\ddot{a}}{c}\\ \frac{\ddddot{f}}{f} &= -\frac{\dddot{a}}{c},\end{aligned} \tag{10}$$

where c is the speed of light, the spin frequency is f, and so on. To compute the values of the apparent frequency derivatives now, we evaluate Equations (8) and (9) at $t=0$ to find

$$\begin{aligned}\frac{\dot{f}}{f} &= \frac{xn_b^2}{c}\sin\omega\\ \frac{\ddot{f}}{f} &= \frac{xn_b^3}{c}\cos\omega\\ \frac{\dddot{f}}{f} &= -\frac{xn_b^4}{c}\sin\omega\\ \frac{\ddddot{f}}{f} &= -\frac{xn_b^5}{c}\cos\omega.\end{aligned} \tag{11}$$

Overall, we find the nth frequency derivative to be

$$f_n = \frac{d^n f}{dt^n} = \frac{f x n_b^{n+1}}{c}(-1)^{n+1}\cos\left(\omega - \frac{n\pi}{2}\right). \tag{12}$$

Note that this differs from Equation (8) in the published article: the $n!$ in the denominator is not present, the signs are flipped, and the dependence on ω is flipped between sin and cos (see Table 1 for an explicit comparison).

The sign swap and the sin/cos swap are not consequential for the conclusions of the published article, since a replacement of $\omega \rightarrow -\omega - \pi/2$ will accomplish that. This means that ω would be redefined but since it is a nuisance variable, it does not change the conclusions. The ratios between successive terms keep the correct behavior.

The lack of $n!$ in the correct terms does change the conclusions slightly, but not qualitatively. For instance, constraints on $\ddot{f} = f_2$ would change by a factor of 2, and using the ratio between successive terms to constrain P_b (Equation (13) of the published article) would be correct except for the removal of $n+1$ in the denominator. The majority of the figures in the published article are essentially unchanged. The exception is Figure 4 (a revised Figure 4 is presented here). One of the pulsars (PSR J1913+1330) included in that figure cannot be solved using the correct expressions for the frequency derivatives as the signs of the measured

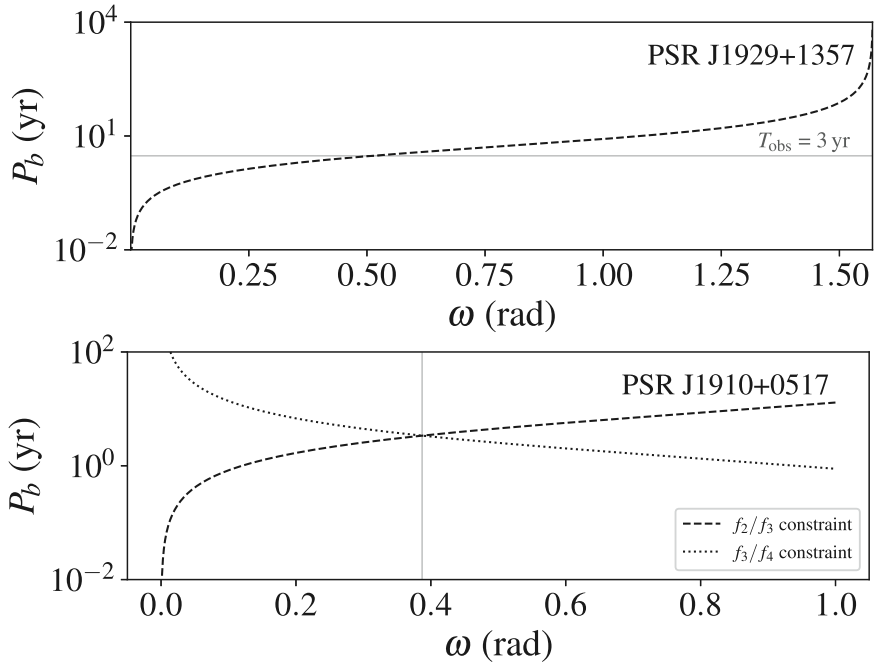

Figure 4. Top: for PSR J1929+1357, instead of allowing $\omega < 0.52$ we find $\omega > 0.52$. Bottom: for PSR J1910+0517 (originally excluded from this figure), we identify a potential solution with $\omega = 0.39 \pm 0.06$ rad and $P_b = 3.4 \pm 0.2$ yr. The published version of this figure also included PSR J1913+1330, but that does not permit a solution as $\ddot{f}$ and $\dddot{f}$ should have the same sign.

$f_2/f_3/f_4$ are not consistent, but one of the pulsars originally excluded is solvable.

We have verified our calculations using a python script to simulate an ELL1 binary and fit it with just frequency derivatives in `PINT` (Luo et al. 2021). The results are consistent with those presented here.

Acknowledgments

We thank an anonymous referee for helpful suggestions. This work was supported by the NANOGrav NSF Physics Frontiers Center award numbers 1430284 and 2020265.

Software: PINT (Luo et al. 2021).

ORCID iDs

Megan L. Jones https://orcid.org/0000-0001-6607-3710
David L. Kaplan https://orcid.org/0000-0001-6295-2881
Maura A. McLaughlin https://orcid.org/0000-0001-7697-7422
Duncan R. Lorimer https://orcid.org/0000-0003-1301-966X

References

Joshi, K. J., & Rasio, F. A. 1997, ApJ, 479, 948
Lange, C., Camilo, F., Wex, N., et al. 2001, MNRAS, 326, 274
Lorimer, D. R., & Kramer, M. 2012, Handbook of Pulsar Astronomy (Cambridge: Cambridge Univ. Press)
Luo, J., Ransom, S., Demorest, P., et al. 2021, ApJ, 911, 45